

Nanoscale

Accepted Manuscript



This is an *Accepted Manuscript*, which has been through the Royal Society of Chemistry peer review process and has been accepted for publication.

Accepted Manuscripts are published online shortly after acceptance, before technical editing, formatting and proof reading. Using this free service, authors can make their results available to the community, in citable form, before we publish the edited article. We will replace this *Accepted Manuscript* with the edited and formatted *Advance Article* as soon as it is available.

You can find more information about *Accepted Manuscripts* in the [Information for Authors](#).

Please note that technical editing may introduce minor changes to the text and/or graphics, which may alter content. The journal's standard [Terms & Conditions](#) and the [Ethical guidelines](#) still apply. In no event shall the Royal Society of Chemistry be held responsible for any errors or omissions in this *Accepted Manuscript* or any consequences arising from the use of any information it contains.

Cite this: DOI: 10.1039/xxxxxxxxxx

Graphene-porphyrin single-molecule transistors[†]

Jan A. Mol,^{*a‡} Chit Siong Lau,^{a‡} Wilfred J. M. Lewis,^b Hatf Sadeghi,^c Cecile Roche,^b Arjen Cnossen,^b Jamie H. Warner,^a Colin J. Lambert,^c Harry L. Anderson,^b and G. Andrew D. Briggs^a

Received Date
Accepted Date

DOI: 10.1039/xxxxxxxxxx

www.rsc.org/journalname

We demonstrate a robust graphene-molecule-graphene transistor architecture. We observe remarkably reproducible single electron charging, which we attribute to insensitivity of the molecular junction to the atomic configuration of the graphene electrodes. The stability of the graphene electrodes allow for high-bias transport spectroscopy and the observation of multiple redox states at room-temperature.

Single molecules have long been heralded as the ultimate form of electronic device scaling.^{1,2} Harnessing the intrinsic functionality of individual molecules enables the bottom-up fabrication of atomically identical electronic building blocks.^{3–6} Contacting single molecules is a serious difficulty in single molecule electronics, because it requires scaleable and robust atomic-size electrodes that are energetically aligned with the molecular orbitals.⁷ A variety of fabrication approaches have been developed, including mechanical⁸ and electromigrated⁹ break-junctions and scanning probe techniques.¹⁰ Single-molecule rectifiers,³ transistors⁴ and switches⁵ have been experimentally demonstrated, and the read-out and manipulation of a single-molecule nuclear spin has been achieved.⁶ Despite these successful approaches the robustness and reproducibility of single-molecule contacts has remained an issue.¹¹ Due to variability in their contacts, break-junction and scanning-probe approaches often rely on the repeated formation of thousands of metal-molecule junctions to infer information on the electronic properties of a single molecule.¹²

Carbon-based electrodes are appealing for contacting individ-

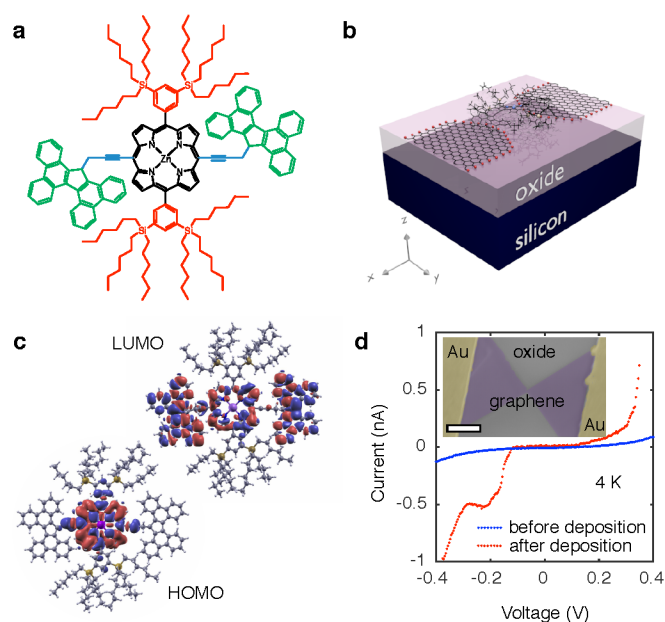


Fig. 1 (a) Chemical structure of the molecular wire with a zinc-porphyrin backbone (black), 'butterfly' anchor groups (green) and bulky side groups (red). The functional groups allow for a robust, self-aligning mechanism. (b) Schematic of the single-molecule transistor. A heavily doped silicon chip with a 300 nm silicon oxide layer is used as a back gate to modulate charge transport through the device. (c) DFT simulations of LDOS for HOMO and LUMO iso-surfaces. (d) Typical 4 K current–voltage ($I-V$) trace before (blue) and after (red) depositing molecules. The observed increase in current after exposing the nanogaps to the porphyrin solution is representative for all devices measured. The inset shows a false-color scanning electron micrograph of the device. The scale bar is 1 μm .

^a Department of Materials, University of Oxford, 16 Parks Road, Oxford OX1 3PH, UK

^b Department of Chemistry, University of Oxford, Chemistry Research Laboratory, Mansfield Road, Oxford OX1 3TA, UK

^c Quantum Technology Centre, Physics Department, Lancaster University, LA1 4YB Lancaster, UK

* jan.mol@materials.ox.ac.uk

[†] Electronic Supplementary Information (ESI) available: [details of any supplementary information available should be included here]. See DOI: 10.1039/b000000x/

[‡] These authors contributed equally to this work

ual molecules.^{13,14} Unlike gold, which is the archetypal electrode materials for metal-molecule junctions, graphene has a low atomic mobility at room temperature, resulting in atomically stable electrodes.¹⁵ While different metals with a lower atomic mobility might also provide stable electrodes,¹⁶ the workfunction of these metals are typically not well matched to the discrete energy levels of the molecule as is the case for graphene.¹⁷ Furthermore, the two-dimensional nature of graphene results in weaker screening of a gate electric field compared to bulky three-dimensional electrodes, which means the distance between the gate electrode can be much larger than the distance between the source and drain electrodes whilst still maintaining the capability of gating the molecular orbitals. Here we demonstrate a robust graphene-molecule-graphene contacting geometry where a stable and reproducible single-molecule single-electron transistor (SET) architecture is achieved through careful design of the molecular building blocks and controlled formation of graphene nanogaps.

Modular molecular designs, consisting of a molecular backbone with specific side-groups for anchoring, spacing and self-alignment, in combination with graphene electrodes, have been proposed to overcome the variability issues that have long limited single-molecule electronics.^{7,18} Orbital gating of small molecules anchored to graphene electrodes has been demonstrated,¹⁵ but, to date, there are no studies of charge transport through complex modular molecules coupled to graphene electrodes. In this work, we study the charge transport through individual molecules in a graphene-molecule-graphene junction. The molecular wire, shown in Figure 1a, consists of a zinc-porphyrin back-bone (black in Figure 1a) with tetrabenzofluorene anchors (green in Figure 1a). Porphyrin molecules provide a versatile platform for molecular device functionality,¹⁹ and have been widely investigated as such.^{20–22} Anchoring the molecular backbone to the graphene electrodes can be achieved either by covalent C-C bonding,²³ or by π – π -stacking.¹⁵ The latter is especially of interest, as it leaves the electronic structure of the molecule largely unchanged, in contrast to thiol anchors which introduce gap-type states.²⁴ Tetrabenzofluorene (TBF) ‘butterfly’ anchor groups used in this study are known to bind strongly to graphite surfaces²⁵ and carbon nanotubes,²⁶ and are robust in solvent solution.²⁵ Density functional theory (DFT) calculations shown in Fig. 1b reveal that there is no steric hindrance to adsorption, and that the molecular wire relaxes across the graphene nanogap in a planar geometry. DFT calculations further indicate that the wavefunctions of the highest occupied molecular orbital (HOMO) are delocalised over the porphyrin backbone and anchor groups in contrast to the lowest unoccupied molecular orbital (LUMO) which are only localised over the porphyrin backbone, as shown in Fig. 1c. Overlap between the delocalised electron wavefunctions of the fully conjugated zinc-porphyrin system with the butterfly anchors allows for electron transport through the wire. The molecular backbone is separated from the butterfly anchor groups by a spacer (blue in Figure 1a), which allows the anchor groups to bind to the defect-free graphene rather than to the graphene edges. In addition to the butterfly limpets, the molecule has two bulky side-groups (red in Figure 1a). The side-groups make the molecular wire more soluble and prevent the central porphyrin from binding to the

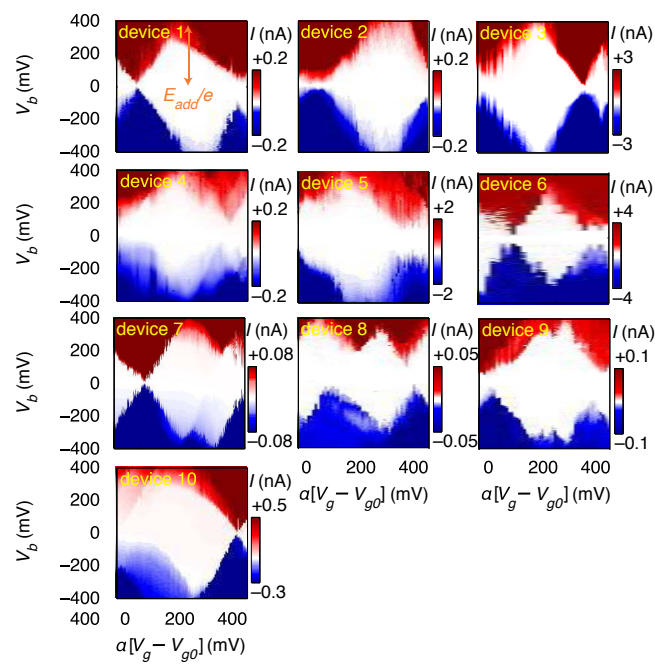


Fig. 2 The source-drain current I as a function of source-drain bias V_b and gate voltage V_g . All devices shown are in the weak-coupling regime where the current $I \sim \text{pA} - \text{nA}$, meaning that an electron tunnels from the source electrode to the molecule, and then on to the drain, in a sequential process. Sequential electron tunnelling leads to diamond shaped regions where charge transport is Coulomb blocked. All devices were measured at 20 mK.

graphene electrodes.

We used lithographically patterned chemical vapour deposited (CVD) single-layer graphene,^{27,28} resulting in devices with greater reproducibility than those fabricated from few-layer graphene flakes.¹⁵ The graphene electrodes are fabricated using feedback-controlled electroburning^{28,29} and are typically separated by 1-2 nm. The chemical potential of the molecular wire is electrostatically tuned using the conducting silicon substrate as a back-gate (see Figure 1b), which is separated from the molecule and graphene electrodes by a 300 nm thick silicon-oxide layer, resulting in a SET device geometry. The graphene electrodes are stable in air for at least several days. Molecules are deposited from a chloroform solution, after which the samples are immediately transferred into vacuum to prevent contamination. Figure 1d shows typical current-voltage traces before (blue) and after (red) deposition of the molecule measured at 4 K. Before deposition of the molecule the current shows smooth exponential behaviour indicative of tunnelling through a single barrier. After deposition the presence of a molecule results in stepwise increases of the current as expected for sequential tunnelling through a double-barrier system. A scanning electron micrograph image of the device is shown in the inset of Fig. 1d.

First, we demonstrate reproducible single-electron transport through individual molecules. We show that the single electron charging is determined by the molecule rather than the microscopic details of the electrodes. Reproducible SET behaviour is measured in 10 out of 48 devices at 20 mK on which we de-

Table 1 Statistics of 68 devices measured at 20 mK. For devices in the column 'no CB' we did not observe any Coulomb peaks at low bias (10 mV), indicating that in these device either no quantum dot is formed, or a quantum dot is formed with an addition energy that exceeds our gate range ($E_{\text{add}} > 0.8$ eV for a gate-coupling $\alpha = 0.01$).

	$E_{\text{add}} < 0.1$	$E_{\text{add}} \approx 0.37$	no CB
TBF anchors	2	10	36
No anchors	0	0	20

113 posited the molecular wire described above, as shown in Fig. 2.
 114 We find that for all devices $E_{\text{add}} = 0.37 \pm 0.05$ eV for the Coulomb
 115 diamond closest to equilibrium (zero gate voltage). The device
 116 statistics presented in Table 1 indicate that the measured SET be-
 117 haviour of the devices shown in Fig. 2 arises from charge trans-
 118 port through approximately identical single-molecule transistors.
 119 In a control experiment using same molecular backbone but with-
 120 out the TBF limpets (see Fig. SI2), 20 devices were tested and
 121 no Coulomb diamonds were observed. From the reproducibility
 122 and from the control experiment we deduce: (i) molecules attach
 123 to the electrodes only when they are functionalised with anchor
 124 groups; (ii) the SET behaviour can be attributed to a molecule
 125 bridging the gap; (iii) the SET behaviour cannot be attributed to
 126 multiple molecules or to random carbon islands. The presence of
 127 multiple molecules would lead to multiple overlapping Coulomb
 128 diamonds whereas carbon islands would be expected to give more
 129 variable energy spacing E_{add} . The observation of a constant en-
 130 ergy spacing of $E_{\text{add}} \approx 0.37$ V for 10 out of 12 of the devices dis-
 131 playing Coulomb diamonds is a clear indication that there is only
 132 one active molecule in each device.

133 A residual degree of variability is still present in the molecu-
 134 lar devices. The horizontal axes in Fig. 2 are scaled by an ef-
 135 fective lever arm α which is a measure of the capacitive cou-
 136 pling between the gate and the molecule, and differs from de-
 137 vice to device, with $\alpha = 0.006 - 0.04$ estimated from the slopes
 138 of the Coulomb diamonds. The gate coupling observed in our
 139 devices with a 300 nm thick oxide are comparable to those re-
 140 ported for metal junctions on an oxide with a thickness of 40
 141 nm.³⁰ The small values of α indicate that the total capacitance is
 142 dominated by the source and drain electrodes, and is consistent
 143 with electrostatic calculations (SI.II.C). The variation in α can
 144 be attributed to differences in screening of the gate-field by the
 145 source and drain electrodes. The gate voltage to align the electro-
 146 chemical potential of the electrodes with the Dirac point is greater
 147 than 40 V, thus giving an upper limit to the shift in the electro-
 148 chemical potential of the electrodes as less than half the change
 149 in the potential of the molecule deduced from the slope of the
 150 Coulomb diamonds (SI.II.D). Trap states in the form of defects in
 151 the gate-oxide that can capture an electron and adsorbants on the
 152 graphene electrodes give rise to shifted and non-closing Coulomb
 153 diamonds (SI.II.E). Finally, we observe a significant variation in
 154 the current through the single-molecule devices, which can be at-
 155 tributed to differences in overlap between the anchor-groups and
 156 the graphene electrodes.

157 By looking more accurately at the transport spectroscopy of de-
 158 vice 8, we can obtain the level spacing of the molecular orbitals²¹⁴

and electron–electron interactions in the molecule. The stability
 of our molecular system (Fig. 3a) allows us to measure the en-
 ergy spacing $E_{\text{add}}(N)$ between the ground state (GS) transitions
 from redox state N to redox state $N + 1$ of the molecule, from
 the height of the Coulomb diamonds. In the constant interaction
 model the addition energy consists of two parts³¹: (i) the charg-
 ing energy E_C , due to the Coulomb interactions among electrons
 in the molecule and between electrons in the molecule and those
 in the environment; and (ii) the gap Δ_{HL} between the HOMO
 and LUMO energy-levels. We can estimate the contribution of
 Δ_{HL} and E_C to the addition energy by comparing $E_{\text{add}}(N)$ for suc-
 cessive redox states and considering the spin-degeneracy of the
 molecular orbitals. We find that $\Delta_{\text{HL}} = 0.05$ eV for the $N - 2$
 redox state and $\Delta_{\text{HL}} = 0.06$ eV for the N redox state. Several redox
 states have been observed in previous work on OPV molecules
 in gold nanogaps.⁴ The interpretation of the different contribu-
 tions to E_{add} can be further substantiated by comparing Δ_{HL} with
 the single-particle energy level spacing which can be determined
 from the excited state spectrum for each redox state (see Fig. 3c).
 The stability of graphene allows us to extend measurements to
 bias-voltages beyond the limit set by electromigration for gold
 electrodes.⁴ We find that the first excited state of the $N - 2$
 redox state aligns closely with the ground state of the $N - 1$
 and N redox states. Likewise, the second excited state of $N - 2$
 redox state aligns with the first excited state of $N - 1$ and N
 and the ground state of the $N + 1$ and $N + 2$ redox states. The single-
 electron energy spectrum seems to be largely independent of the
 number of electrons, with intervals dominated by the HOMO-
 LUMO energy separation. Renormalisation corrections of $\sim 3 - 4$
 eV have been observed experimentally and predicted theoretic-
 ally for molecules in nanogaps³² and for molecules on graphite
 surfaces.³³ For unscreened gas phase molecules our calculations
 yield an addition energy for one electron $E_{\text{add}} = 3.84$ eV. From
 a simple screening potential (see SI.III) we estimate the reduc-
 tion of the addition energy to be of the order of 3 eV, which is in
 reasonable agreement with our experimental findings.

Finally, we discuss the room temperature operation of the
 graphene-molecule-graphene transistors. Fig. 4 shows the sta-
 bility diagram of device 2 measured at room temperature. Two
 Coulomb diamonds can be fully resolved, allowing us to probe
 the charge state transitions between three successive redox states.
 Using the same methodology as describe above we can estimate
 the charging energy $E_C = 0.28 \pm 0.05$ eV and HOMO–LUMO gap
 $\Delta_{\text{HL}} = 0.09 \pm 0.05$ eV by comparing E_{add} of the N and $N + 1$
 redox states measured at room temperature.

In conclusion, we have demonstrated room-temperature
 charge- and energy-quantization in a reproducible graphene-
 molecule-graphene device geometry. The modular design of the
 molecular wire makes this approach applicable to a wide variety
 of molecular backbones. Specifically, the $\pi - \pi$ anchoring of the
 molecule to the highly stable graphene nano-electrodes allows
 high-bias energy spectroscopy of the excited states and removes
 the need for statistical analysis of ensemble measurements. Our
 findings offer a route to a vast number of quantum transport ex-
 periments that are well established for semiconductor quantum
 dots, but at an energy-scale larger than kT at room temperature.

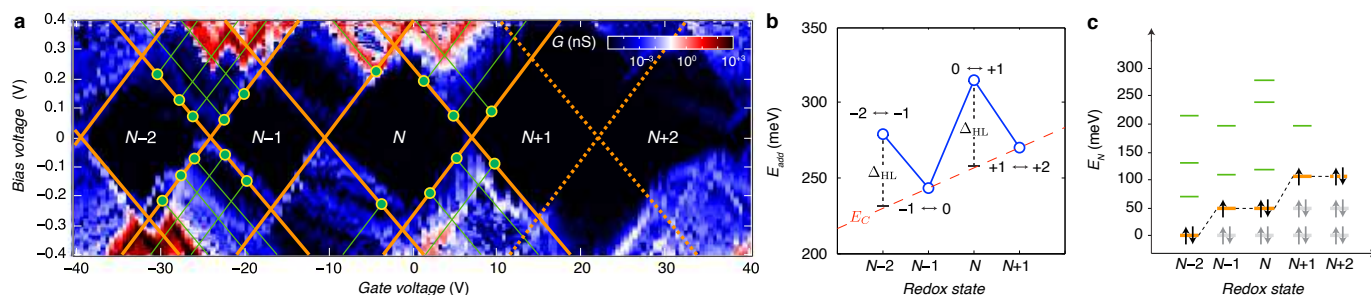


Fig. 3 (a) Differential conductance dI/dV_g (on a logarithmic scale) as a function of V_b and V_g . The excited state spectrum is measured from the source/drain conductance. Excited state transitions result in lines in the differential conductance diagram running parallel to the edges of the Coulomb diamonds. The bias voltage where an excited state line intersects the Coulomb blockade region (indicated by the green dots in a) is a direct measure of the excited state energy $E_{N,i} = e|V_{b,i}|$, where $E_{N,i}$ is the energy of i th excited state with respect to the ground state for the N th redox state. The $N+1 \leftrightarrow N+2$ transition appears to be suppressed (dashed lines), the charge degeneracy point for this transition is inferred from the features in the bottom-right of the $N+1$ diamond and the top-left of the $N+2$ diamond. (b) Addition energy as a function of the redox state N . The HOMO–LUMO gap Δ_{HL} is estimated from the energy difference in odd-even filling. For a redox state with an even number of electrons in the molecule, the HOMO is fully occupied and the additional electron will occupy the LUMO which is separated from the HOMO by the single-particle energy-level spacing Δ_{HL} . We identify the two high-energy transitions as the even \leftrightarrow odd transitions where $E_{add}(N) = E_C + \Delta_{HL}$ and the low-energy as the odd \leftrightarrow even transitions where $E_{add}(N) = E_C$. The charging energy $E_C(N) = E_{C0} + \beta N$ with $E_{C0} = 0.23$ eV $\beta = 0.01$ eV is estimated from a linear interpolation of $E_{add}(N-1)$ and $E_{add}(N+1)$. (c) Single-particle energy spectrum as a function of redox state N . Using the values for Δ_{HL} and the excited state spectra for each redox state an orbital-filling diagram is constructed. Starting from the $N-2$ redox state, the successive ground state energy level is found by adding Δ_{HL} , resulting in the orange lines in c. Next the excited state energies $E_{N,i}$ are added to the ground state energy for each redox state, resulting in the green lines in c.

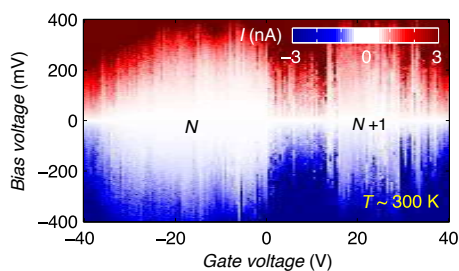


Fig. 4 Current stability diagram as a function of V_b and V_g measured at room temperature. We attribute the shift in the Coulomb diamonds with respect to the 20 mK data to thermal activation of offset charges in the oxide.

An approach that combines single molecules with novel two-dimensional materials and semiconductor fabrication technologies forms an attractive platform with which to realise scalable room-temperature single-electron transistor networks. Such an architecture could consist of individual molecules coupled to each other via graphene leads, with nearby graphene gate-electrodes to tune the orbital energy levels of the individual molecules. The gate-electrodes could be separated from the molecules by a two-dimensional insulator, to enable strong capacitive coupling between the gate and the molecule and allow the single-molecule transistors to exhibit gain. Here we have demonstrated the first step towards such an architecture: a reproducible single-molecule transistor. Further improvements in the graphene nanogap fabrication need to be made to reduce the offset charges and eliminate variability in the gate coupling as discussed above, providing a basis for the development of single-molecule electronics and also applicable to the fabrication of single-molecule based sensors and spin-based quantum computation.

234

235

Acknowledgements We thank the Royal Society for a Newton International Fellowship for J.A.M. and a University Research Fellowship for J.H.W., and the Agency for Science Technology and Research (A*STAR) for a studentship for C.S.L. This work is supported by Oxford Martin School, EPSRC grants EP/J015067/1, EP/K001507/1, EP/J014753/1, EP/H035818/1, and the European Union Marie-Curie Network MOLESCO. This project/ publication was made possible through the support of a grant from Templeton World Charity Foundation. The opinions expressed in this publication are those of the author(s) and do not necessarily reflect the views of Templeton World Charity Foundation.

246

References

- 1 A. Aviram and M. A. Ratner, *Chemical Physics Letters*, 1974, **29**, 277–283.
- 2 S. V. Aradhy and L. Venkataraman, *Nature Nanotechnology*, 2013, **8**, 399–410.
- 3 R. M. Metzger, B. Chen, U. Höpfner, M. V. Lakshminathan, D. Vuillaume, T. Kawai, X. Wu, H. Tachibana, T. V. Hughes, H. Sakurai, J. W. Baldwin, C. Hosch, M. P. Cava, L. Brehmer and G. J. Ashwell, *Journal of the American Chemical Society*, 1997, **119**, 10455–10466.
- 4 S. Kubatkin, A. Danilov, M. Hjort, J. Cornil, J.-L. Brédas, N. Stuhr-Hansen, P. Hedegård and T. Bjørnholm, *Nature*, 2003, **425**, 698–701.
- 5 S. Y. Quek, M. Kamenetska, M. L. Steigerwald, H. J. Choi, S. G. Louie, M. S. Hybertsen, J. B. Neaton and L. Venkataraman, *Nature Nanotechnology*, 2009, **4**, 230–234.
- 6 S. Thiele, F. Balestro, R. Ballou, S. Klyatskaya, M. Ruben and W. Wernsdorfer, *Science*, 2014, **344**, 1135–1138.
- 7 E. Lörtscher, *Nature Nanotechnology*, 2013, **8**, 381–384.
- 8 C. Bruot, J. Hihath and N. Tao, *Nature Nanotechnology*, 2011, **7**, 35–40.
- 9 W. Liang, M. P. Shores, M. Bockrath, J. R. Long and H. Park, *Nature*, 2002, **417**, 725–729.
- 10 C. M. Guédon, H. Valkenier, T. Markussen, K. S. Thygesen, J. C. Hummelen and S. J. van der Molen, *Nature Nanotechnology*, 2012, **7**, 305–309.
- 11 G. Schull, T. Frederiksen, A. Arnau, D. Sánchez-Portal and R. Berndt, *Nature Nanotechnology*, 2010, **6**, 23–27.
- 12 B. Xu, *Science*, 2003, **301**, 1221–1223.
- 13 X. Guo, J. P. Small, J. E. Klare, Y. Wang, M. S. Purewal, I. W. Tam, B. H. Hong, R. Caldwell, L. Huang, S. O'Brien, J. Yan, R. Breslow, S. J. Wind, J. Hone, P. Kim and C. Nuckolls, *Science*, 2006, **311**, 356–359.
- 14 C. W. Marquardt, S. Grunler, A. Baszczyk, S. Dehm, F. Hennrich, H. von Löh-

- 274 neysen, M. Mayor and R. Krupke, *Nature Nanotechnology*, 2010, **5**, 863–867.
275 15 F. Prins, A. Barreiro, J. W. Ruitenberg, J. S. Seldenthuis, N. Aliaga-Alcalde,
276 L. M. K. Vandersypen and H. S. J. van der Zant, *Nano Letters*, 2011, **11**, 4607–
277 4611.
278 16 F. Prins, T. Hayashi, B. J. A. de Vos van Steenwijk, B. Gao, E. A. Osorio, K. Muraki
279 and H. S. J. van der Zant, *Applied Physics Letters*, 2009, **94**, 123108.
280 17 C. Jia and X. Guo, *Chemical Society Review*, 2013, **42**, 5642.
281 18 C. G. Péterfalvi and C. J. Lambert, *Phys. Rev. B*, 2012, **86**, 085443.
282 19 M. L. Perrin, F. Prins, C. A. Martin, A. J. Shaikh, R. Eelkema, J. H. van Esch,
283 T. Briza, R. Kaplanek, V. Kral, J. M. van Ruitenbeek, H. S. J. van der Zant and
284 D. Dulić, *Angewandte Chemie International Edition*, 2011, **50**, 11223–11226.
285 20 M. Jurow, A. E. Schuckman, J. D. Batteas and C. M. Drain, *Coordination Chem-*
286 *istry Reviews*, 2010, **254**, 2297–2310.
287 21 S. Mohnani and D. Bonifazi, *Coordination Chemistry Reviews*, 2010, **254**, 2342–
288 2362.
289 22 G. Sedghi, V. M. Garcia-Suarez, L. J. Esdaile, H. L. Anderson, C. J. Lambert,
290 S. Martin, D. Bethell, S. J. Higgins, M. Elliott, N. Bennett, J. E. Macdonald and
291 R. J. Nichols, *Nat Nano*, 2011, **6**, 517–523.
292 23 Y. Cao, S. Dong, S. Liu, L. He, L. Gan, X. Yu, M. L. Steigerwald, X. Wu, Z. Liu
293 and X. Guo, *Angewandte Chemie International Edition*, 2012, **51**, 12228–12232.
294 24 M. L. Perrin, C. J. O. Verzijl, C. A. Martin, A. J. Shaikh, R. Eelkema, J. H. van
295 Esch, J. M. van Ruitenbeek, J. M. Thijssen, H. S. J. van der Zant and D. Dulić,
296 *Nature Nanotechnology*, 2013, **8**, 282–287.
297 25 J. K. Dutton, J. H. Knox, X. Radisson, H. J. Ritchie and R. Ramage, *Journal of*
298 *the Chemical Society, Perkin Transactions 1*, 1995, 2581.
299 26 M. Assali, M. P. Leal, I. Fernández, P. Romero-Gomez, R. Baati and N. Khier,
300 *Nano Research*, 2010, **3**, 764–778.
301 27 Y. A. Wu, Y. Fan, S. Speller, G. L. Creeth, J. T. Sadowski, K. He, A. W. Robertson,
302 C. S. Allen and J. H. Warner, *ACS Nano*, 2012, **6**, 5010–5017.
303 28 C. S. Lau, J. A. Mol, J. H. Warner and G. A. D. Briggs, *Physical Chemistry Chemical*
304 *Physics*, 2014, 20398–20401.
305 29 H. Sadeghi, J. A. Mol, C. S. Lau, G. A. D. Briggs, J. Warner and C. J. Lambert,
306 *Proceedings of the National Academy of Sciences*, 2015, **112**, 2658–2663.
307 30 M. L. Perrin, E. Burzurí and H. S. J. van der Zant, *Chem. Soc. Rev.*, 2015, **44**,
308 902–919.
309 31 K. Kaasbjerg and K. Flensberg, *Nano Letters*, 2008, **8**, 3809–3814.
310 32 K. Moth-Poulsen and T. Bjørnholm, *Nature Nanotechnology*, 2009, **4**, 551–556.
311 33 J. B. Neaton, M. S. Hybertsen and S. G. Louie, *Phys. Rev. Lett.*, 2006, **97**, 216405.